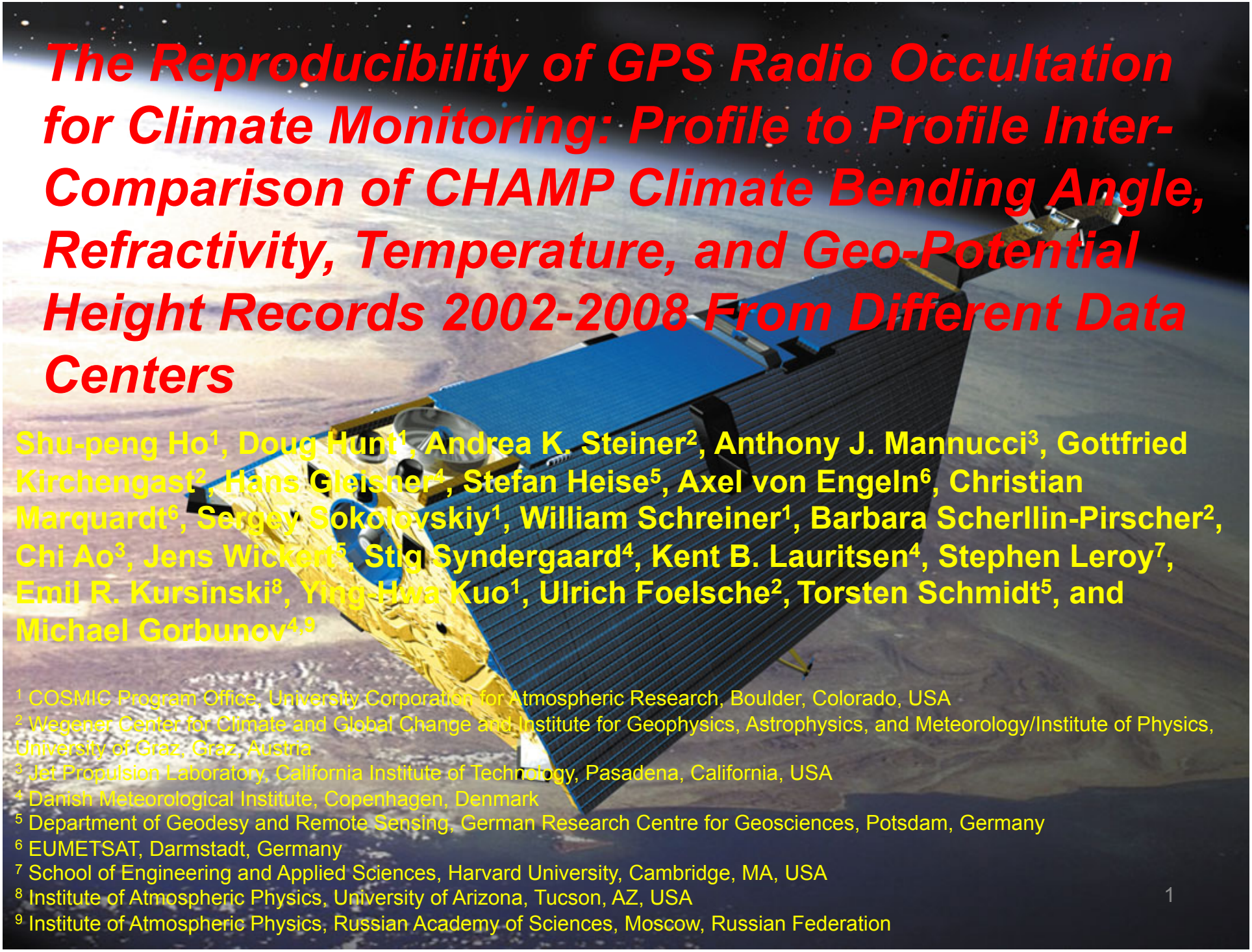

The Reproducibility of GPS Radio Occultation for Climate Monitoring: Profile to Profile Inter-Comparison of CHAMP Climate Bending Angle, Refractivity, Temperature, and Geo-Potential Height Records 2002-2008 From Different Data Centers

Shu-peng Ho[1], Doug Hunt[1], Andrea K. Steiner[2], Anthony J. Mannucci[3], Gottfried Kirchengast[2], Hans Gleisner[4], Stefan Heise[5], Axel von Engeln[6], Christian Marquardt[6], Sergey Sokolovskiy[1], William Schreiner[1], Barbara Scherllin-Pirscher[2], Chi Ao[3], Jens Wickert[5], Stig Syndergaard[4], Kent B. Lauritsen[4], Stephen Leroy[7], Emil R. Kursinski[8], Ying-Hwa Kuo[1], Ulrich Foelsche[2], Torsten Schmidt[5], and Michael Gorbunov[4,9]

[1] COSMIC Program Office, University Corporation for Atmospheric Research, Boulder, Colorado, USA
[2] Wegener Center for Climate and Global Change and Institute for Geophysics, Astrophysics, and Meteorology/Institute of Physics, University of Graz, Graz, Austria
[3] Jet Propulsion Laboratory, California Institute of Technology, Pasadena, California, USA
[4] Danish Meteorological Institute, Copenhagen, Denmark
[5] Department of Geodesy and Remote Sensing, German Research Centre for Geosciences, Potsdam, Germany
[6] EUMETSAT, Darmstadt, Germany
[7] School of Engineering and Applied Sciences, Harvard University, Cambridge, MA, USA
[8] Institute of Atmospheric Physics, University of Arizona, Tucson, AZ, USA
[9] Institute of Atmospheric Physics, Russian Academy of Sciences, Moscow, Russian Federation

1. Motivation:

1) Current long-term measurements used to generate climate data records are mainly derived from satellite observations
2) Quality of satellite measurements/retrievals depend on calibration/retrieval algorithms (and on the a priori profile and atmospheric/surface conditions).
3) GPS RO data for climate monitoring: Raw observation is SI traceable, high vertical resolution, insensitive to clouds and precipitation. While the fundamental phase measurement is synchronized to the ultra-stable atomic clocks on the ground, the RO-derived variables (e.g., refractivity, pressure, temperature) are not.

What are the structural uncertainties for using GPS RO data for climate monitoring ?

And how the structural uncertainties propagate in the inversion chain ?

AIRS Degree Freedom of Signal

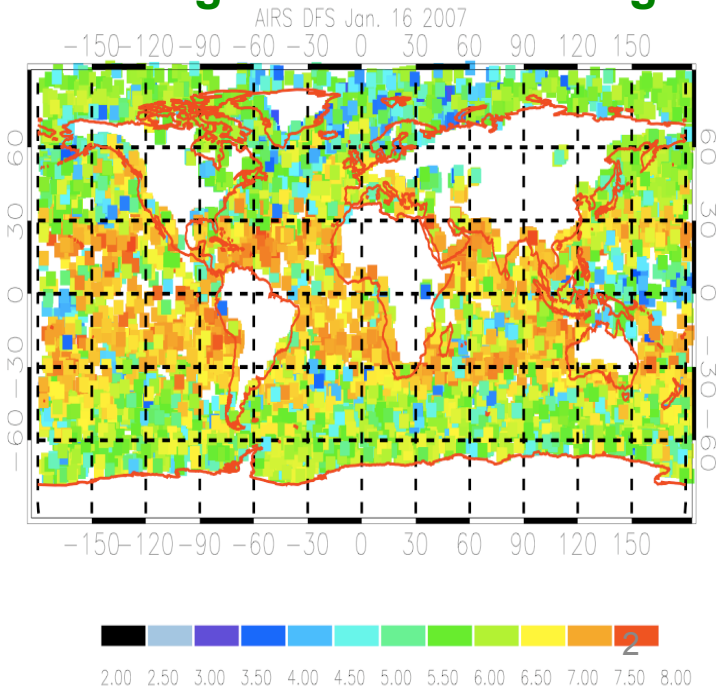

2. Outlines :

- Challenges to use satellite data to define/validate a global trend
- Introduction of RO inversion algorithm
- Compare RO derived variables generated from different centers

3. Conclusions and Future Work

Shu-peng Ben Ho, UCAR/COSMIC

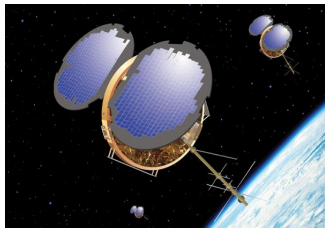

Challenges to use satellite data to define/validate a global trend

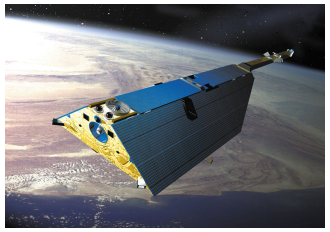

Satellites: Comparability and Reproducibility ?

1) Not designed for climate monitoring

2) Changing platforms and instruments

(No Comparability)

a. Satellite dependent bias, b. geo-location dependent bias, c. orbital drift dependent bias

3) Different processing/merging method lead to different trends (RSS vs. UAH).

(No Reproducibility)

Radiosondes: changing instruments and observation practices; limited spatial coverage especially over the oceans.

We need measurements with high precision, high accuracy, long term stability, reasonably good temporal and spatial coverage as climate benchmark observations.

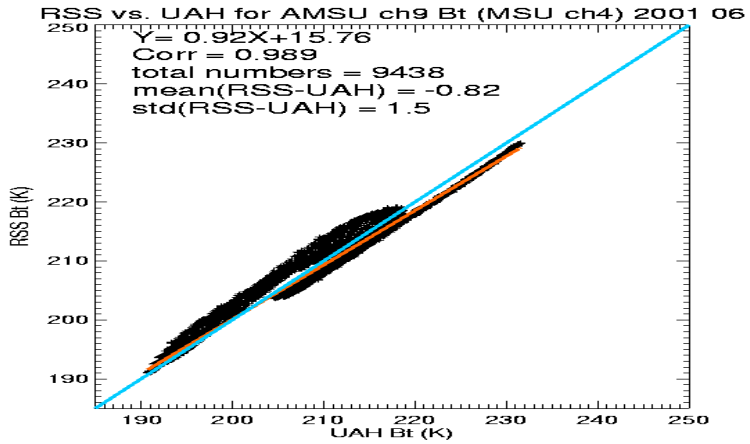

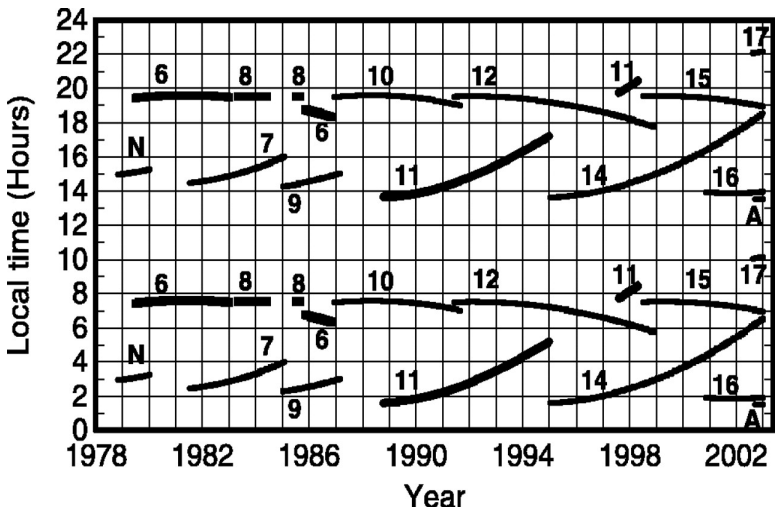

Shu-peng Ben Ho, UCAR/COSMIC

AIRS temperature retrievals depend on the a priori profile and atmospheric/surface conditions, vertical resolution, and also the retrieval methods

$$T_{AIRS}^{\mathrm{Re}t} = A_{AIRS} T_{True} + (I - A_{AIRS}) T_{AIRS}^{Apr}$$

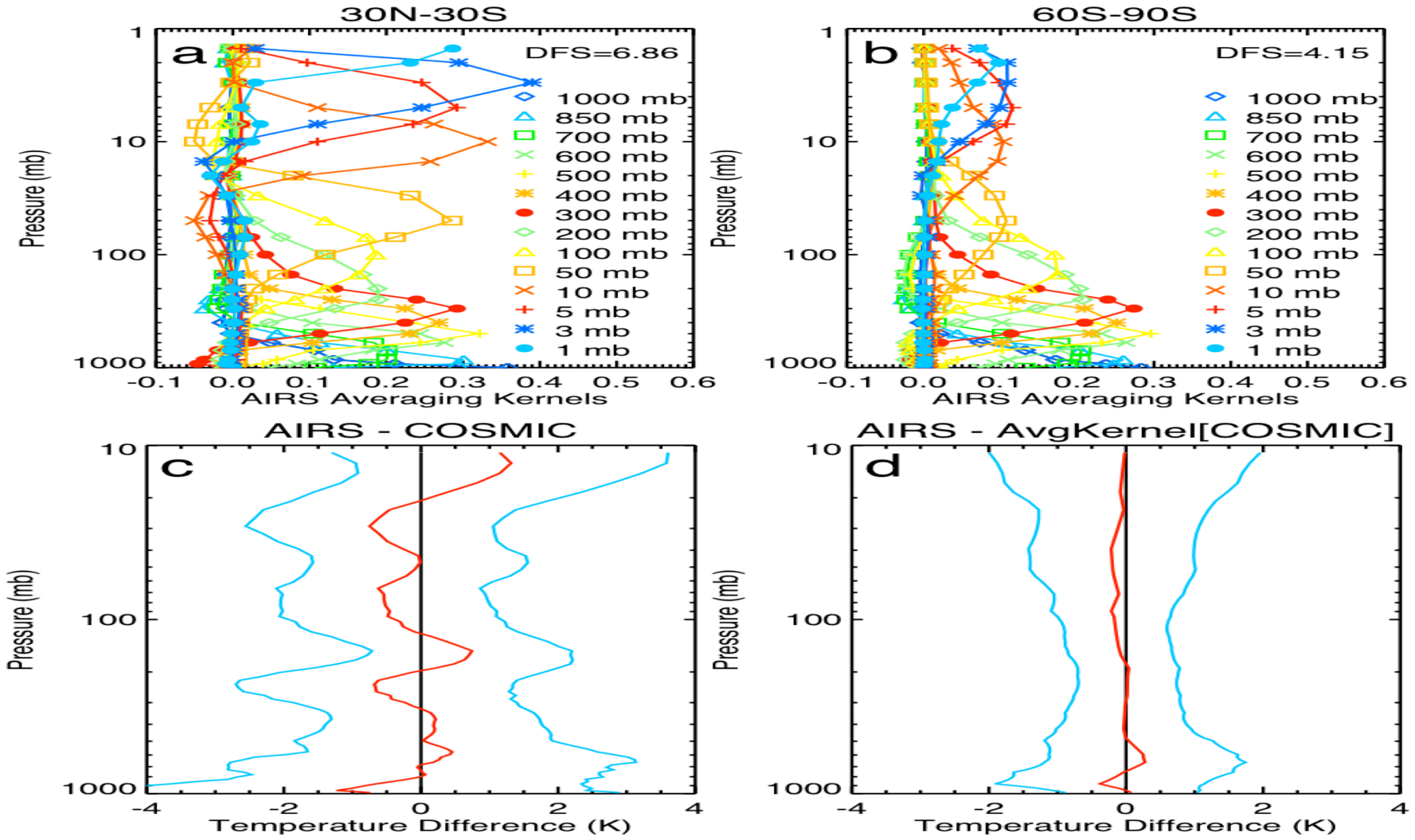

Inversion procedures for RO data

Accurate RO retrievals of atmospheric variable profiles depend on the adequate calculation of the GPS excess atmospheric phase data of two L band frequencies (1575.42 MHz (L1) and 1227.6 MHz (L2)) due to signal delay and bending in the Earth's atmosphere and ionosphere

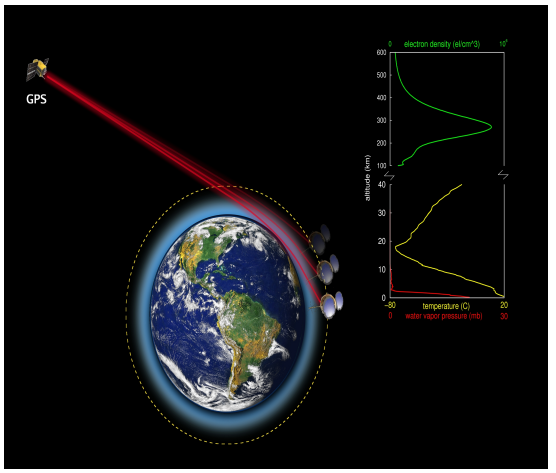

1. RO atmospheric excess phase processing,
2. POD and clock synchronization,
3. The procedure to retrieve bending angle from the Doppler measurement,
4. The extrapolation of the ionospheric correction into the lower troposphere, necessary because of the influence of the ionosphere on measured phase delay of GPS signals,
5. The initialization of the Abelian integral transform to convert atmospheric bending angles to profiles of refractivity,
6. The procedure to derive dry temperature and dry pressure, which are obtained in the upper troposphere by assuming a completely dry atmosphere,
7. The procedure to derive geo-potential height, and
8. Quality control procedures for above steps.

DMI, EUM, WEGC use the RO excess phase processed by UCAR

Uncertainty introduced by inversion procedures :Assumption, simplification and approximations are used in the RO inversion procedures.

Overview on implementations of processing chains at DMI, EUM, GFZ, JPL, UCAR, and WEGC.

URL/ Processing step	Implementations for each center
URL	**DMI :** *http://www.romsaf.org* **EUM** : *http://www.eumetsat.int* **GFZ** : *http://isdc.gfz-potsdam.de* **JPL** : *http://genesis.jpl.nasa.gov* **UCAR**: *http://www.cosmic.ucar.edu* **WEGC**: *http://www.wegcenter.at/globclim*
POD phase and orbit data	**DMI :** UCAR CDAAC orbit and phase data used (version 2009.2650). **EUM :** UCAR CDAAC orbit and phase data used (version 2009.2650). **GFZ** : POD: EPOS-OC for Rapid Science Orbit provision (König et al. 2006); Excess Phase: Single differencing, reference link smoothing. **JPL** : POD: reduced-dynamic strategy using GIPSY software (Bertiger et al.,1994); Excess Phase: Double differencing. **UCAR**: POD computed with Bernese 5.0 software (Dach et al., 2007); Excess Phase: Single differencing, reference link smoothing. **WEGC**: UCAR CDAAC orbit and phase data used (version 2009.2650).
Bending angle calculation	**DMI:** Canonical Transfrom (CT2) inversion [*Gorbunov and Lauritsen*, 2004] below 25 km, combined with GO used above 25 km. **EUM:** Geometric optics used for BAs at all heights **GFZ** : Full Spectrum Inversion (FSI) below 15 km (Jensen et al., 2003); Geometric optics used above 15 km. **JPL** : Canonical transform (CT) after Gorbunov (2002) applied to L1. **UCAR**: FSI (Jensen et al., 2003) applied to L1 in troposphere < dynamic L2 QC height; Geometric optics used > dynamic L2 QC height. **WEGC**: Geometric optics used for L1 and L2 BAs at all heights.
Ionospheric correction	**DMI:** Optimal linear combination of L1 and L2 BAs [*Vorob'ev and Krasil'nikova*, 1994; Gorbunov, 2002]; Iono. correction term extrapolation < dynamic L2 QC height. Linear combination of L1 and L2 BAs [*Vorob'ev and Krasil'nikova*, 1994]. **EUM:** Linear combination of L1 and L2 BAs (Vorob'ev and Krasil'nikova, 1994). **GFZ** : Linear combination of L1 and L2 BAs (Vorob'ev and Krasil'nikova, 1994), **JPL** : Linear comb. of L1 and L2 BAs (Vorob'ev and Krasil'nikova, 1994); Iono. correction term extrapolation below 10 km. **UCAR**: Linear comb. of L1 and L2 BAs (Vorob'ev and Krasil'nikova, 1994); Iono. correction term extrapolation < dynamic L2 QC height. **WEGC**: Linear comb. of L1 and L2 BAs (Vorob'ev and Krasil'nikova, 1994); Iono. correction term extrapolation < 15 km.
Initialization of bending angles	**DMI:** Optimization after Gorbunov (2002), but using a two-parameter fit of background (MSISE-90) to data above 40 km in combination with a global background search (Lauritsen et al., 2011). Dynamic estimation of obs. errors (Gorbunov, 2002); background error fixed at 50%. **EUM:** Using simplified optimal interpolation for bending angle smoothing *Sokolovskiy and Hunt* [1996]. Extension of bending angles up to 150km using CIRA-MSIS climatology; smoothed transition to climatology over 1.5km. **GFZ** : Optimization after Sokolovskiy and Hunt (1996) with MSISE-90 (> 40 km). **JPL** : Exponential function fit at 40–50 km and extrapolation above. **UCAR**: Optimization after Sokolovskiy and Hunt (1996) with fitting backgr. prof. (NCAR clim. extrap. to 150 km), dynamic estimation of the top fit height, background and obs. errors (Lohmann 2005). **WEGC** Numerical integration over bending angle (Simpson's trapezoidal rule) from each height (impact par.) to 120 km. Impact par. to height conversion with radius of curvature at mean TP location [*Syndergaard*, 1998]; Sinc-windowed Blackman filter on refractivity (< 1 km moving average, for resolution-conserving filtering of residual numerical processing noise).
Derivation of refractivity	**DMI:** Numerical calculation of the Abel integral [*Fjeldbo et al.*, 1971] from each height to 150 km. **GFZ** : Abel inversion of the optimized bending angle profiles starts at 150 km.. **JPL** : Able inversion of the ionosphere-corrected bending angle from each height up to 120 km. **UCAR**: The optimized bending angle is subjected to Abel inversion below 150 km by applying the finite-difference representation (*Sokolovskiy et al.*, 2005). **WEGC**: Statistical optimization > 30 km with ECMWF analyses and MSISE-90 to 120 km (Healy, 2001), dynamic estimation of obs. errors and inverse covariance weighting (Gobiet and Kirchengast, 2004; Gobiet et al., 2007).
Dry air retrieval	**DMI:** Refractivity is directly proportional to air density (applying ideal gas equation). Pressure downward integration of the hydrostatic equation from 150 km (boundary conditions determined from the refractivity and its gradient at the top); Dry geopotential height relative to EGM-96; Temperature: Smith-Weintraub formula for dry air [*Smith and Weintraub*, 1953]. **GFZ** : Pressure retrieval is initialized at 100 km with MSISE-90. Pressure downward integration using hydrostatic equation. ; Dry geopotential height relative to EGM-96; Dry temperature after Smith-Weintraub eq. and eq. of state. **JPL** : Pressure integration using hydrostatic equation starting at 40 km. Dry geopotential height relative to JGM-3. Dry temperature after Smith-Weintraub eq. and eq. of state, temperature initialization using ECMWF temperature at 40 km.

Approaches to quantify structural uncertainties among centers:

- Using CHAMP data from 2002 to 2008
- Collecting CHAMP data processed by DMI, EUM, JPL, GFZ, UCAR, WEGC
- Matching Profile-to-profile (common set) of GPS RO derived bending angle, refractivity, temperature, pressure and geo-potential height profiles from individual centers (monthly mean climatologies including a different number of profiles per center, Ho et al., 2009)
- Differences and standard deviations of the individual centers relative to the inter-center mean are used to quantify the structural uncertainty (sampling error due to temporal and spatial mismatches is not an issue in this study).

Matching Profile-to-profile (common set) of GPS RO from six centers

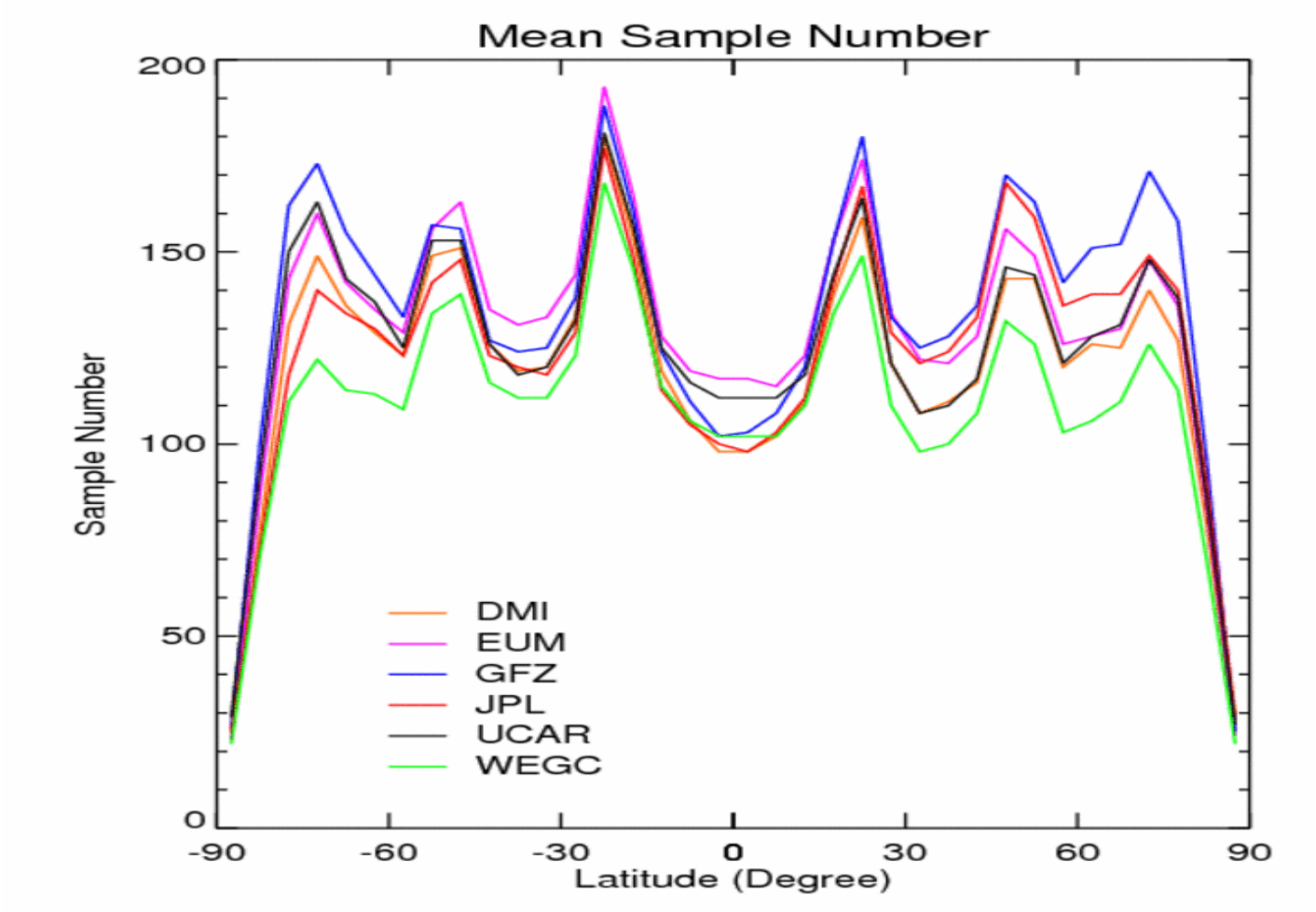

Monthly mean number of sampling in lat bin of 5 degree at 20 km altitude for the year 2007.

Global PPC statistics : UCAR – inter-center Mean from 2002 – 2008

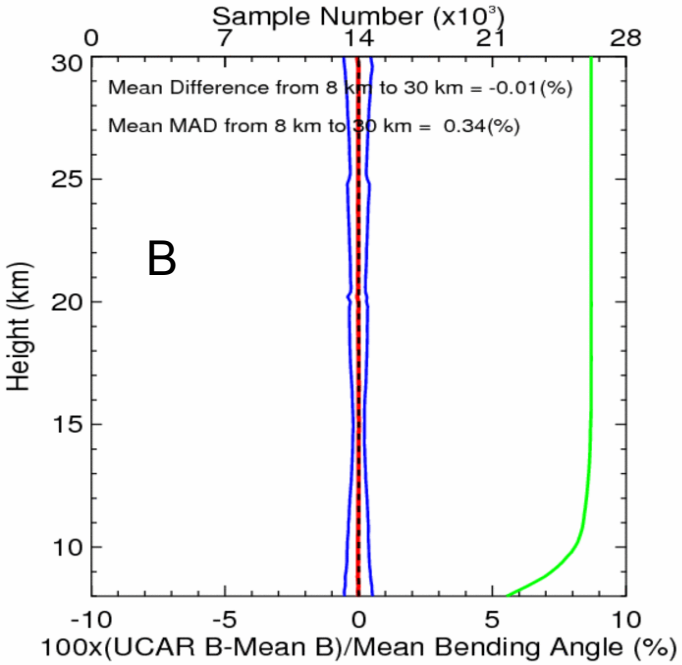

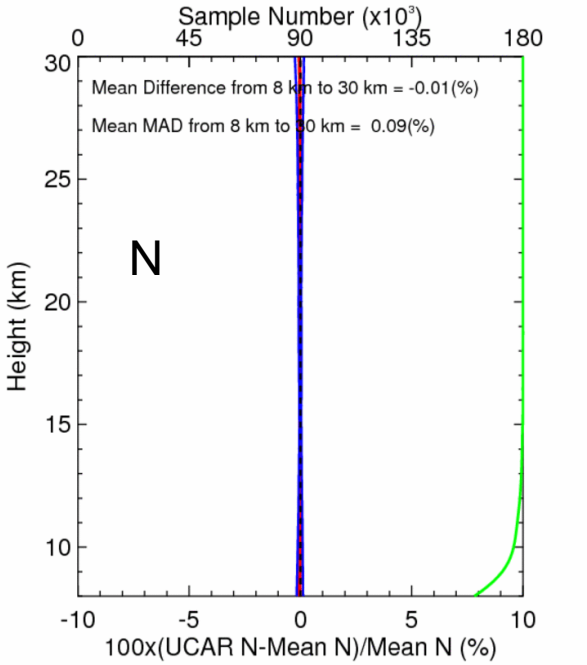

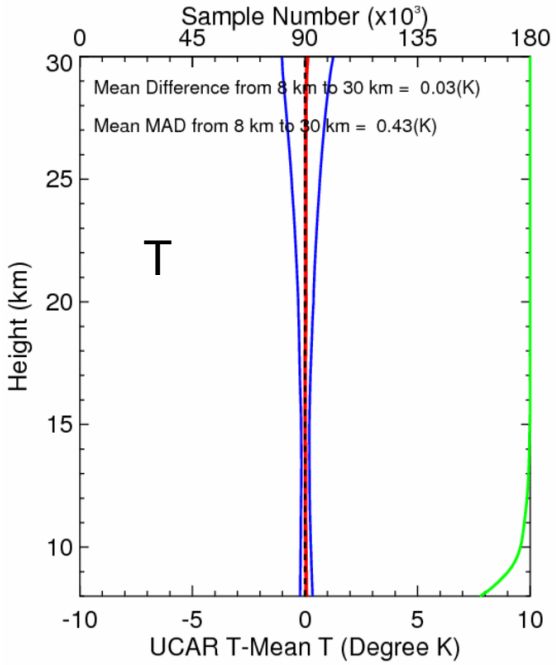

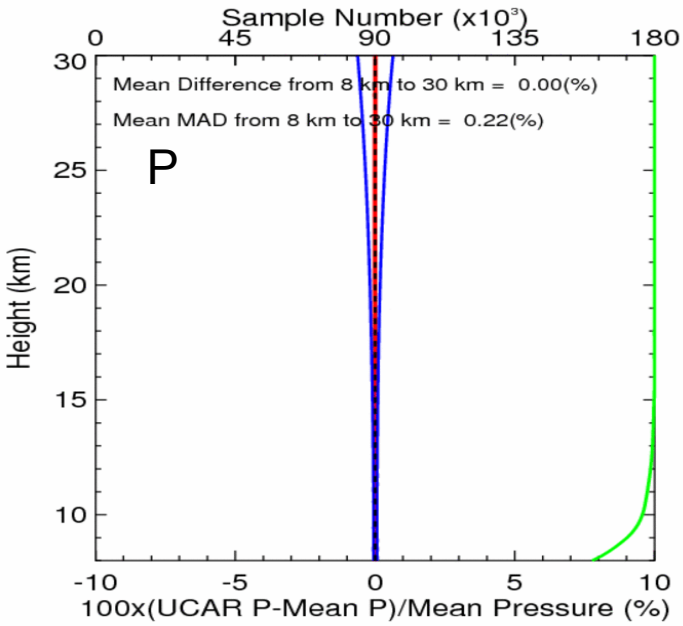

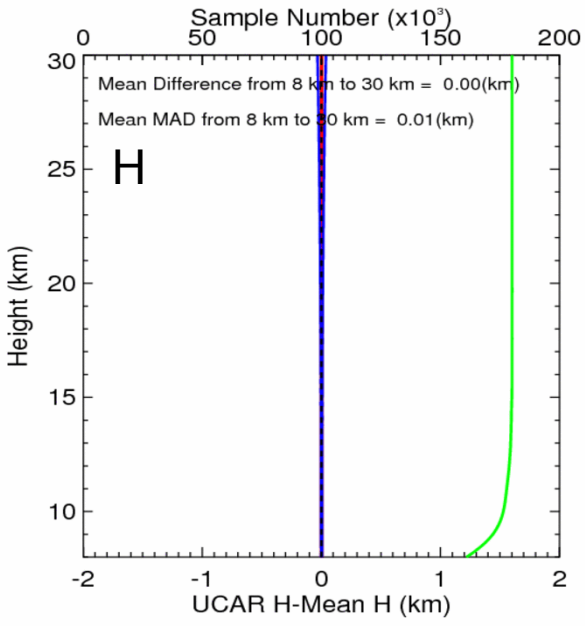

B: -0.01 ± 0.34%
N : -0.01±0.09%
T : 0.03 ± 0.43K
P : 0.00± 0.22%
H : 2 ± 13 m

Temperature error estimated by PPC and simulation study

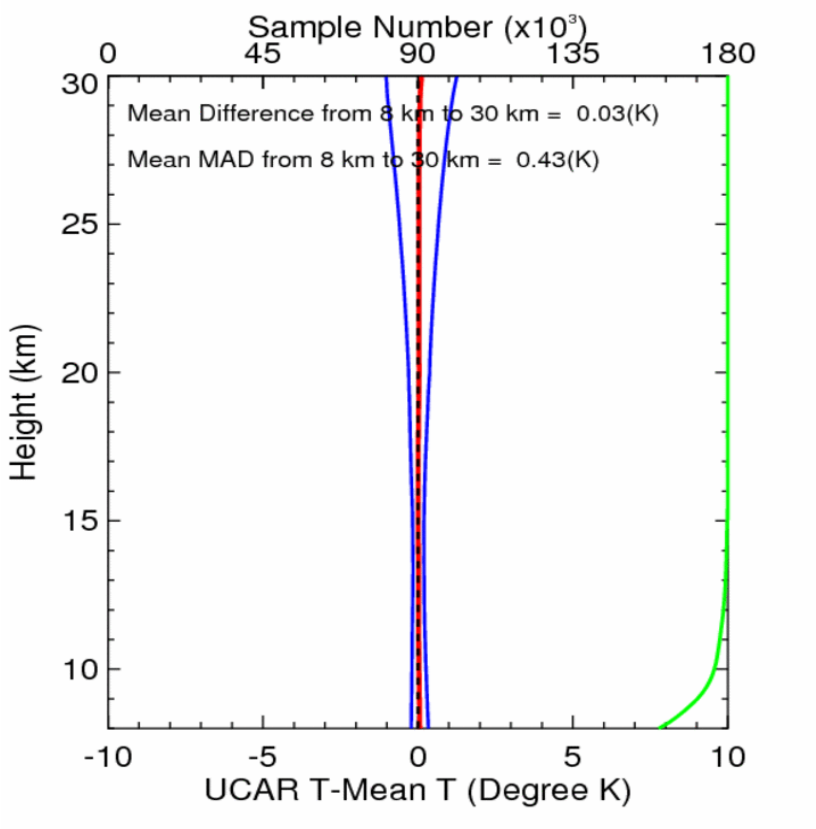

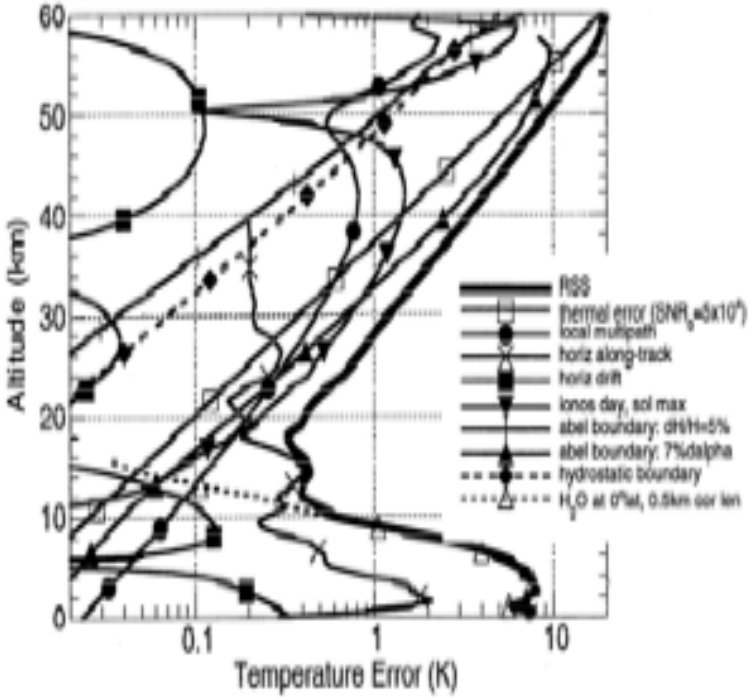

Temperature error estimated by Kursinski 1997 (Figure 12)

Difference in the mean zonal-average fractional refractivity for 2007 among five centers

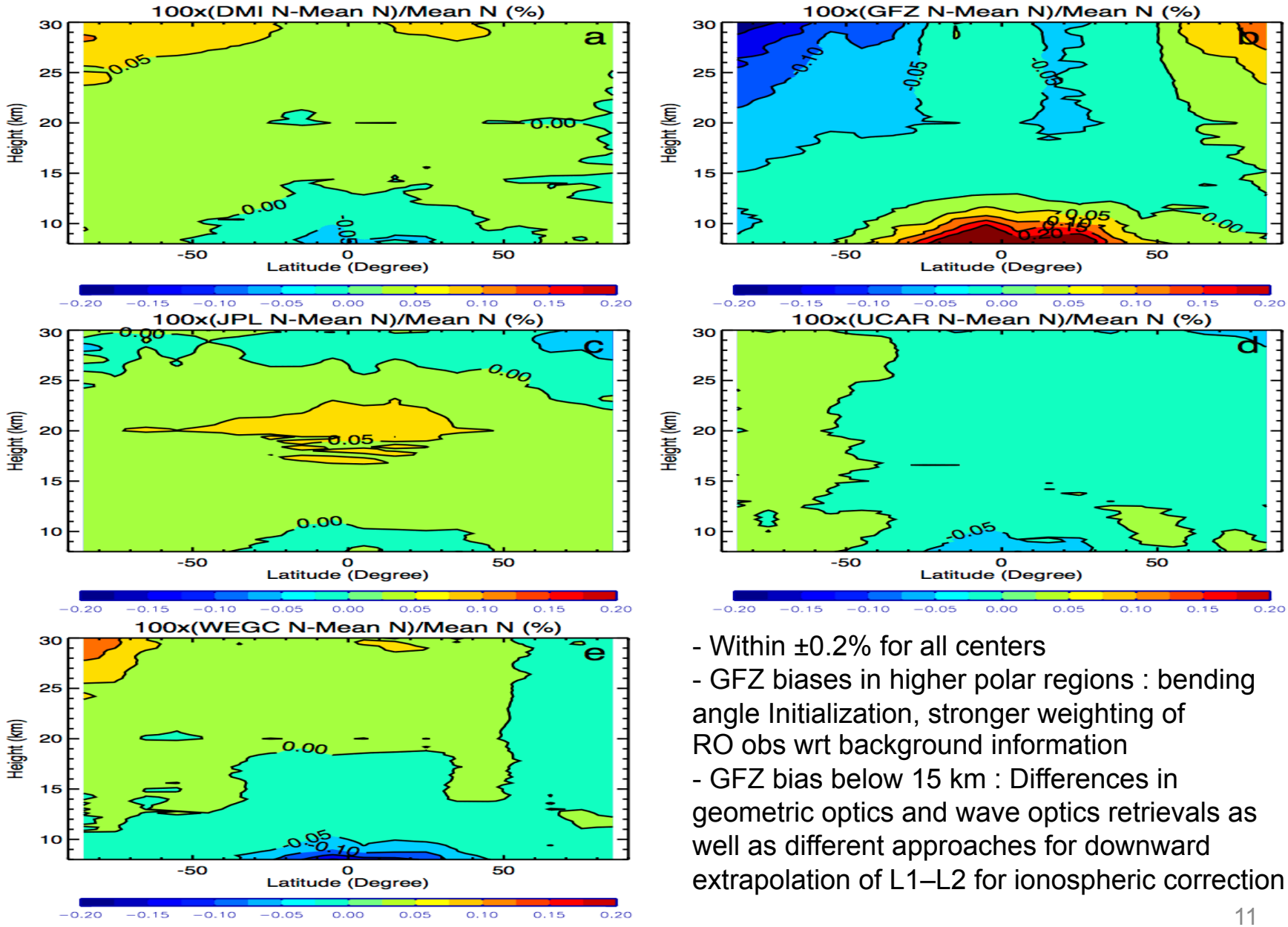

- Within ±0.2% for all centers
- GFZ biases in higher polar regions : bending angle Initialization, stronger weighting of RO obs wrt background information
- GFZ bias below 15 km : Differences in geometric optics and wave optics retrievals as well as different approaches for downward extrapolation of L1–L2 for ionospheric correction

Difference in the mean zonal-average temperature for 2007 among five centers

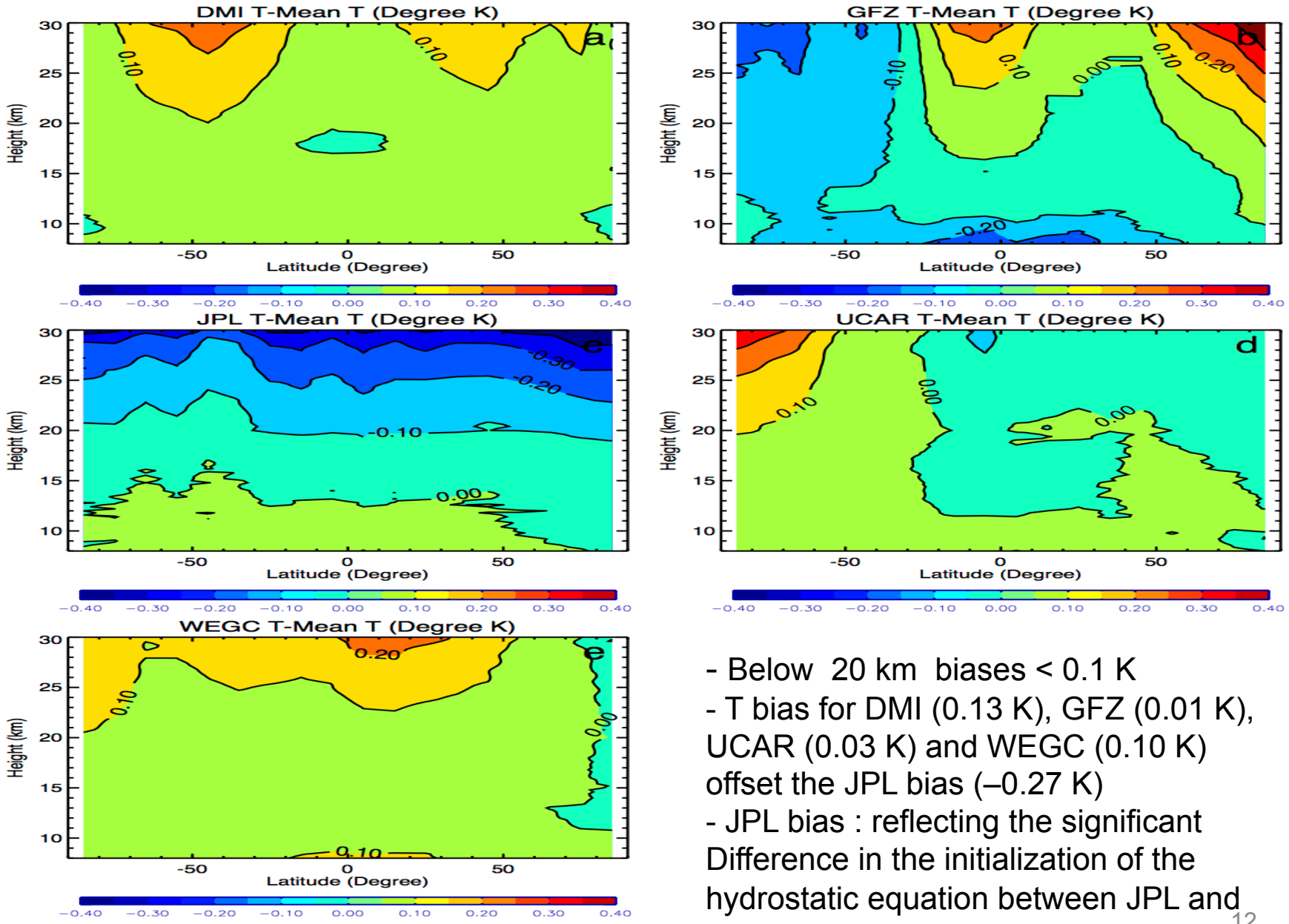

- Below 20 km biases < 0.1 K
- T bias for DMI (0.13 K), GFZ (0.01 K), UCAR (0.03 K) and WEGC (0.10 K) offset the JPL bias (–0.27 K)
- JPL bias : reflecting the significant Difference in the initialization of the hydrostatic equation between JPL and other data centers

The Median Absolute Deviation of the temperature anomalies temperature for 2007 among five centers

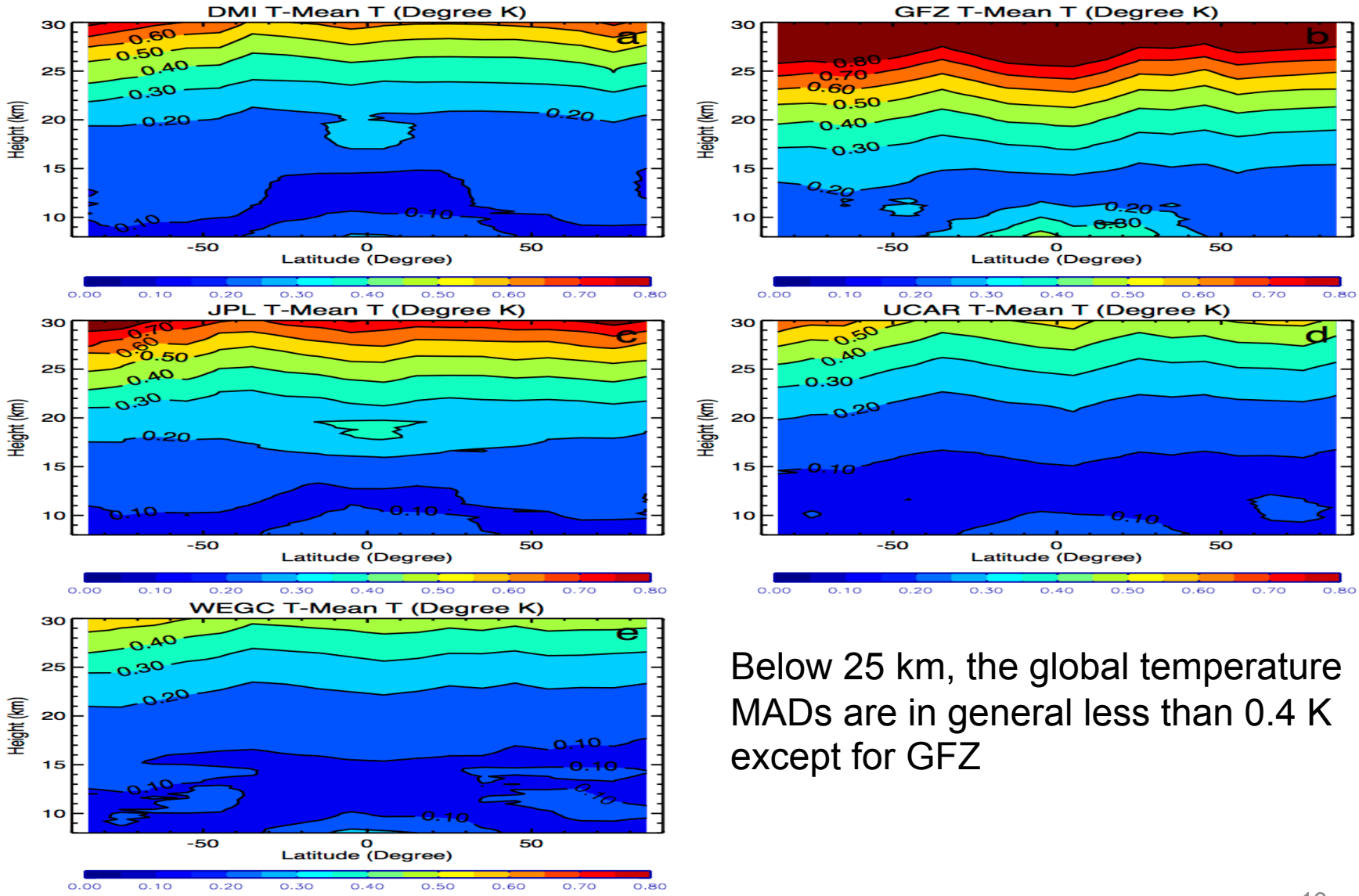

Below 25 km, the global temperature MADs are in general less than 0.4 K except for GFZ

Time Series of (Bending Angle – Mean Bending Angle)/Mean Bending Angle%

8-12km

20-30 km

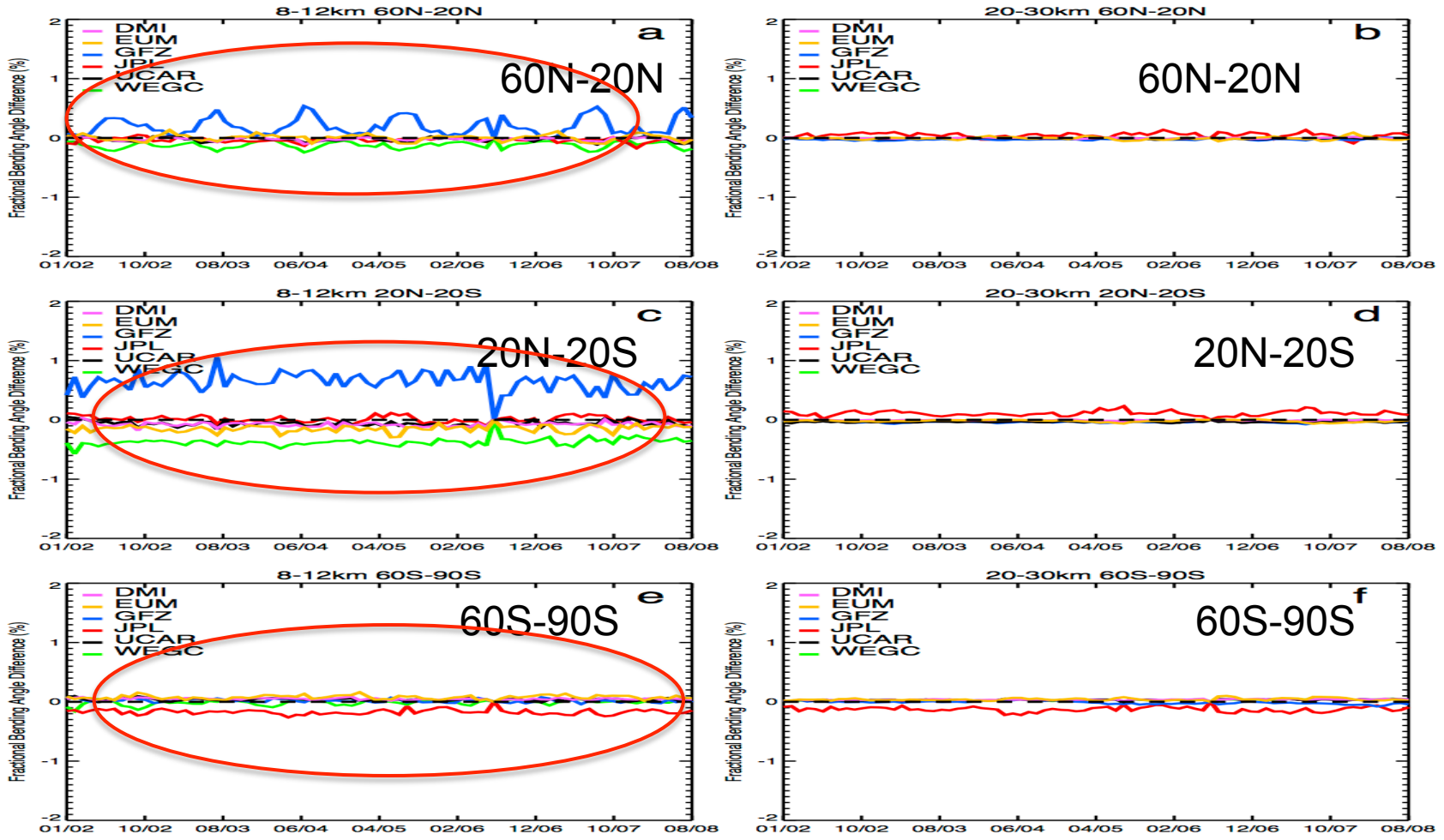

(i) the anomalies from individual centers are persistent in time and there is no obvious latitudinal dependent biases

(ii) individual center's differences show no obvious inter-monthly and inter-seasonally variance

(iii) Mean difference 8 km to 30 km layer are –0.01% (DMI), –0.02%(EUM), 0.12% (GFZ), 0.02% (JPL), –0.02% (UCAR), and –0.08% (WEGC)

Time Series of (Refractivity – Mean Refractivity)/Mean refractivity %

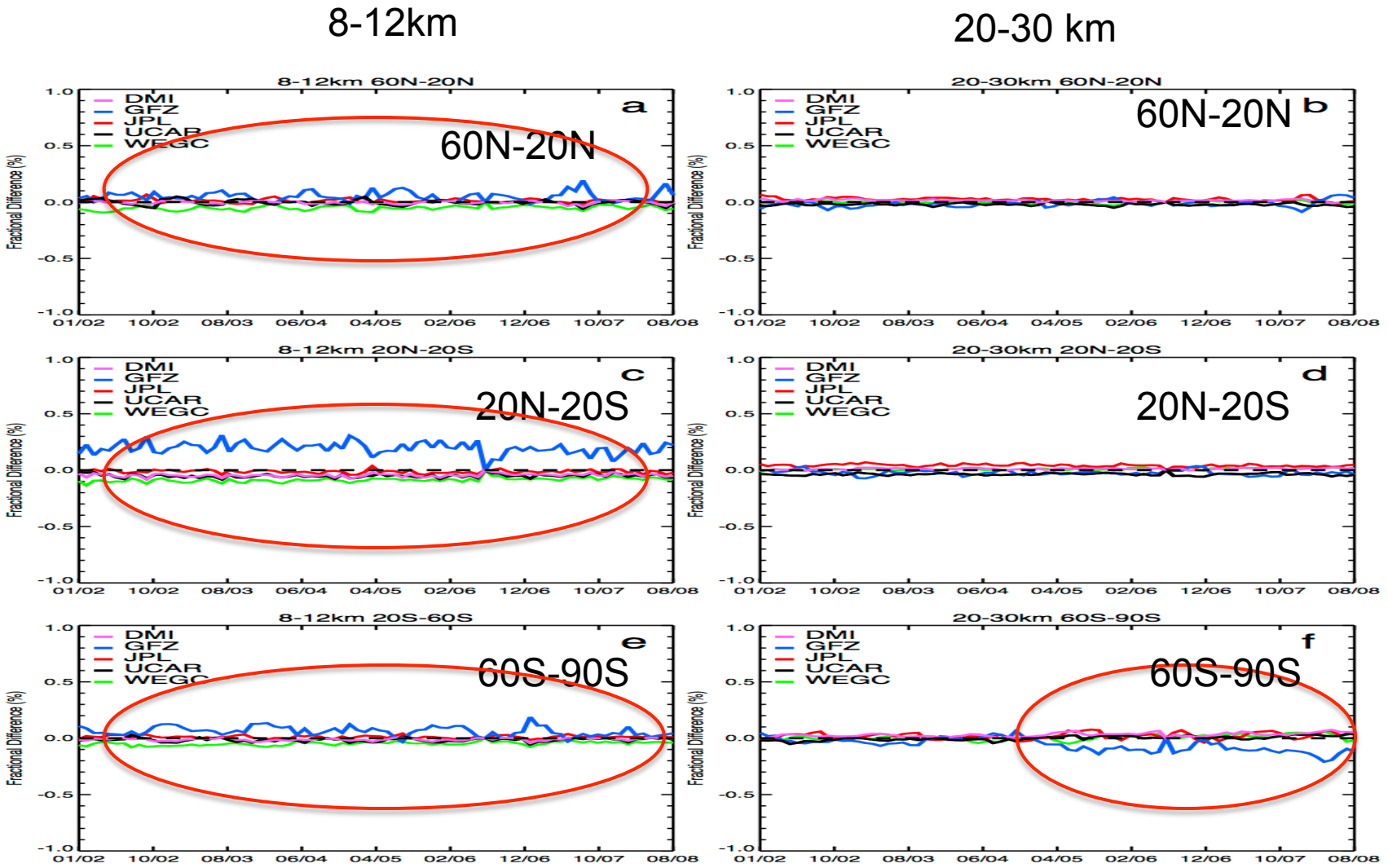

(i) The time series of fractional refractivity differences show similar qualitative features as bending angle but with a different magnitude.

(ii) The mean global differences among centers in the 8 km to 30 km layer are within ±0.03% with about 0.01% standard deviation

Time Series of (Temperature – Mean Temperature) (K)

8-12km

20-30 km

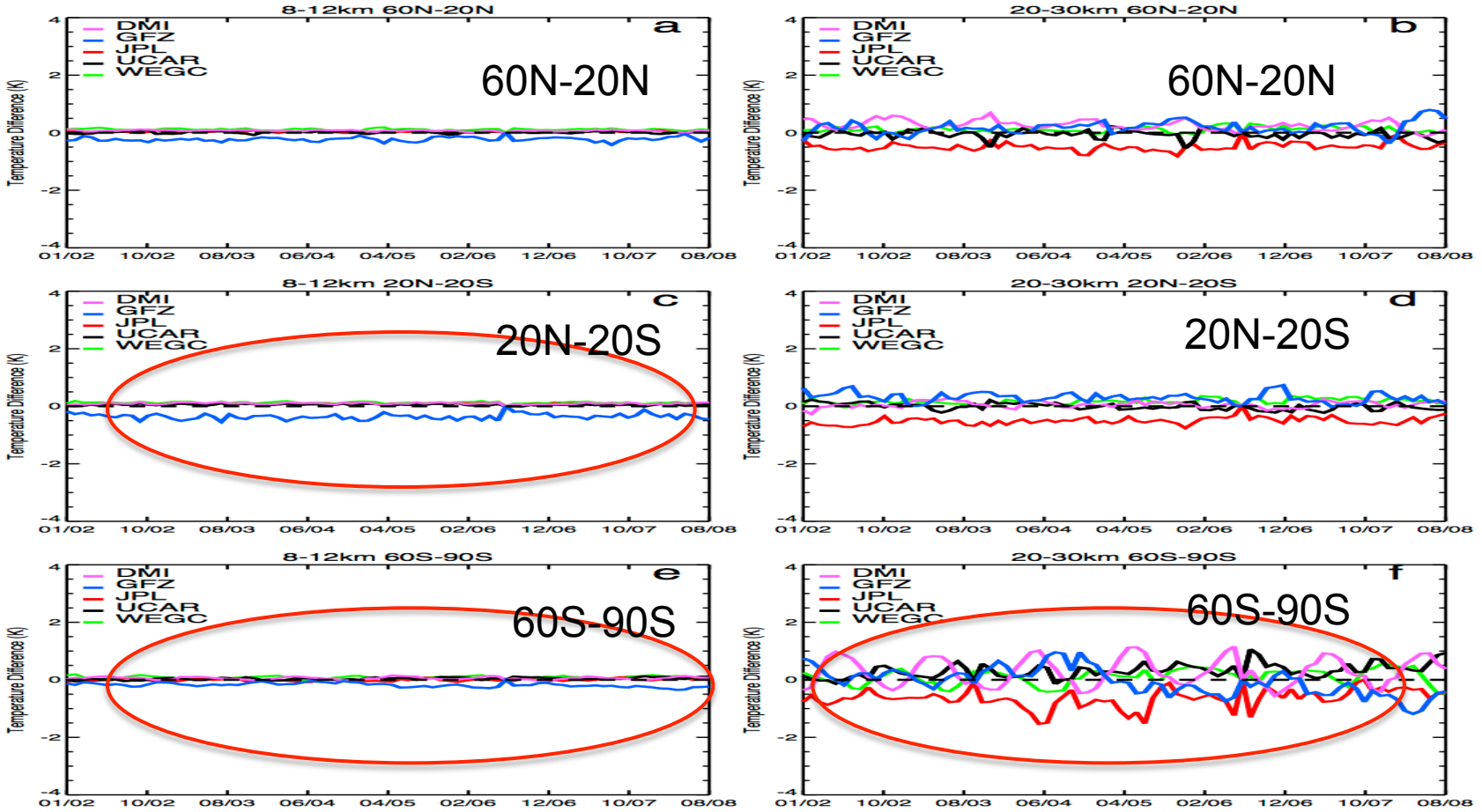

(i) The reason for the obvious inter-seasonal variability in DMI most likely originates from the inability of the MSISE-90 climatology to represent the real stratosphere and mesosphere at high latitudes.

(ii) The mean global difference in LS (20-30 km) are 0.23 K (DMI), 0.15 K (GFZ), –0.55 K (JPL), 0.05 K (UCAR), and 0.12 K (WEGC), respectively, and the corresponding standard deviations are within 0.09 K

De-seasonalized fractional refractivity anomalies for each center

8-12km

20-30 km

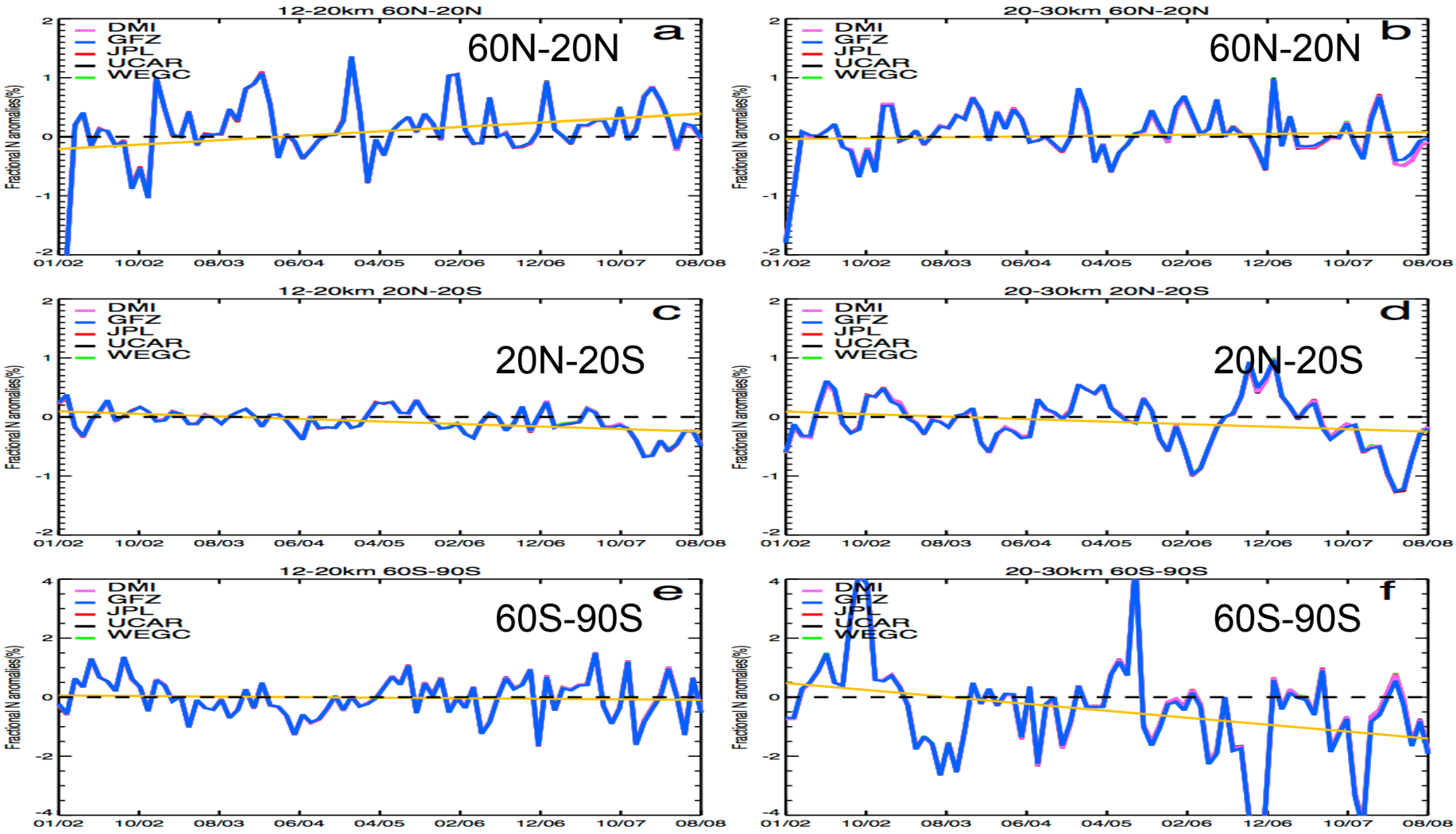

The mean trend differences in the 8 km to 30 km layer for refractivity are within ±0.02%/5yrs

De-seasonalized temperature anomalies for each center

12-20 km

20-30 km

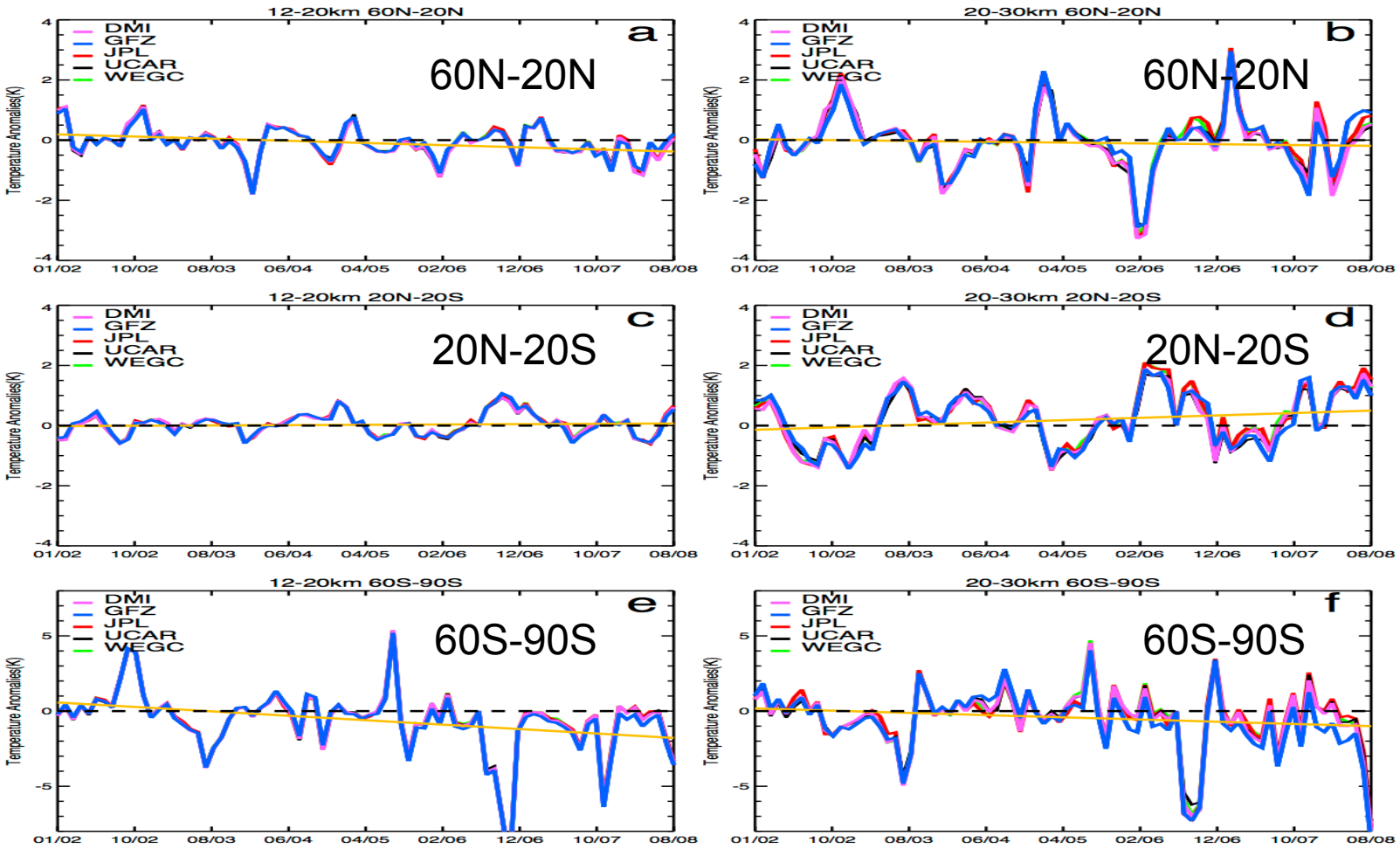

The mean trend differences in the 8 km to 30 km layer for bending angle, refractivity, dry temperature, dry pressure, and dry geopotential height are within ±0.02%/5yrs, ±0.02%/5yrs, ±0.06 K/5yrs, ±0.02%/5yrs, and ±2.3 m/5yrs, respectively.

Difference of De-seasonalized T anomalies to the mean of de-seasonalized T anomalies of all centers

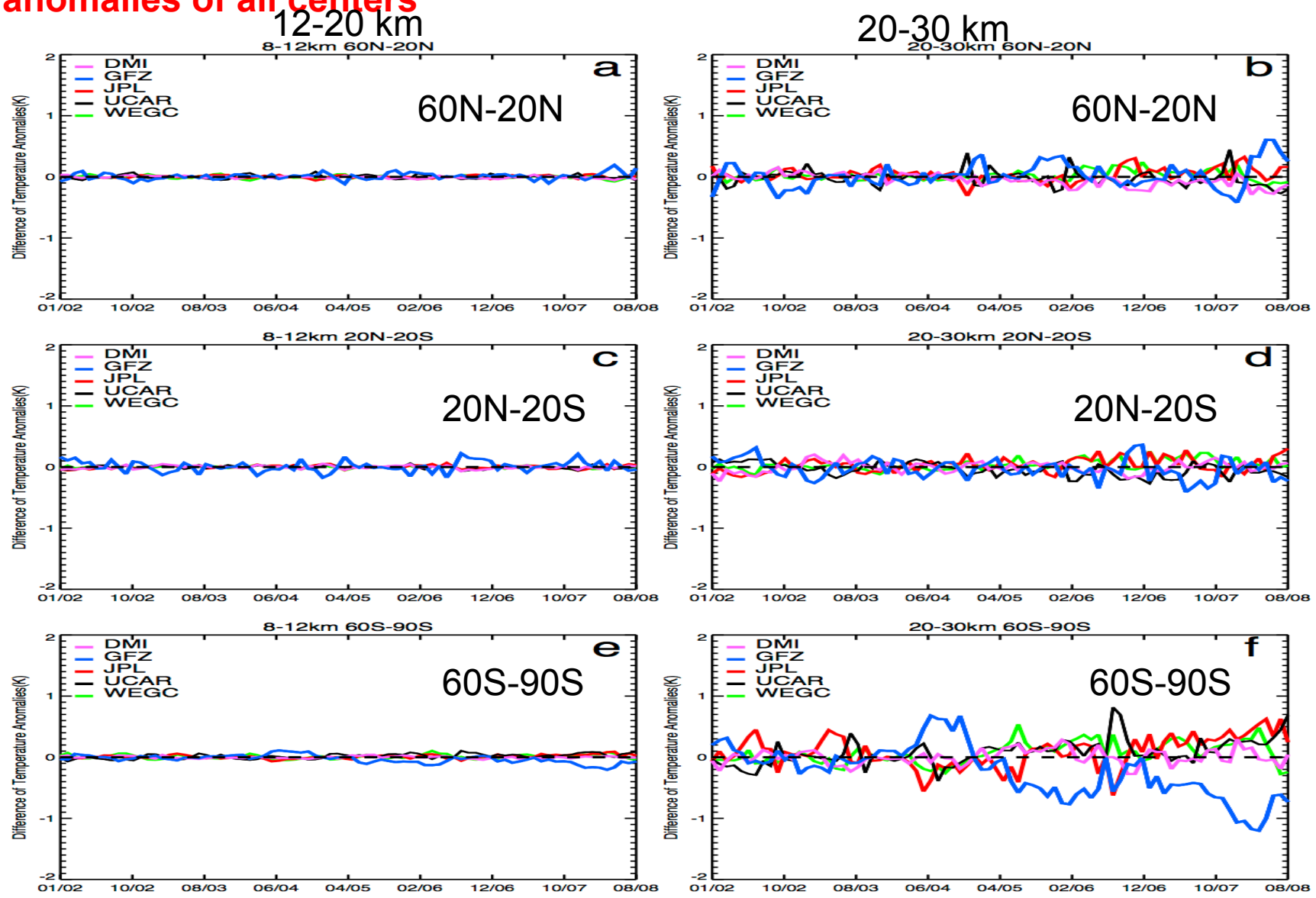

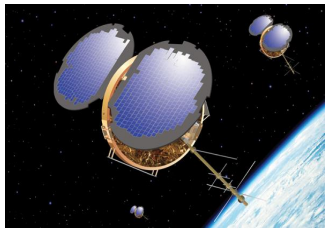

Conclusions

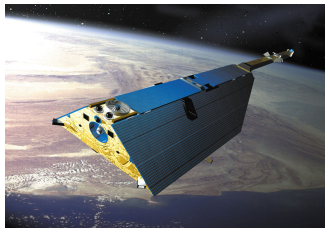

- **Results show that different implementations in the inversion procedures do introduce small but stable retrieval differences among centers. The mean global differences of bending angle, refractivity, dry temperature, dry pressure, and dry geopotential height in the 8 km to 30 km layer for 01/2002 to 08/2008 are between –0.03% and 0.04% (B), –0.01% and 0.02% (N), –0.27 K and 0.13 K (T), –0.11% and 0.07% (P), and –10 m and 10 m (H), respectively.**

- **Although the derived variables from bending angle to temperature and geo-potential height are not readily traceable to SI units, the high precision nature of the raw RO observables is preserved in the inversion chain. The mean standard deviation from all centers near 15 km for bending angle, refractivity, dry temperature, dry pressure, and dry geo-potential height is within 0.5% (B), 0.1% (N), 0.3 K (T), 0.02% (P), and 10 m (H), respectively.**

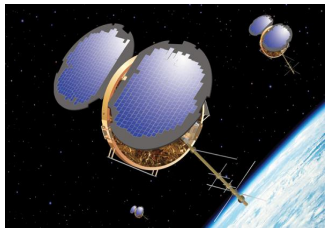

Conclusions

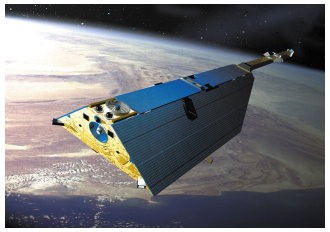

• **Although there are small mean anomaly differences among centers, they are more or less constant in the time series comparisons. The mean anomaly differences of the time series in the 8 km to 30 km layer for bending angle, refractivity, dry temperature, dry pressure, and dry geopotential height for all centers are –0.08% to 0.12% (B), –0.03% to 0.02% (N), –0.27 K to 0.15 K (T), –0.04% to 0.04% (P), and –7.6 m to 6.8 m (H), respectively. The corresponding standard deviation is within 0.02% (B), 0.01% (N), 0.06 K (T), 0.02% (P), and 2.0 m (H), respectively.**

•**With systematic inter-monthly time series anomalies among centers, the trend differences among centers is generally very small. The mean trend differences in the 8 km to 30 km layer for bending angle, refractivity, dry temperature, dry pressure, and dry geopotential height are within ±0.02%/5yrs (B), ±0.02%/5yrs (N), ±0.06 K/5yrs (T), ±0.02%/5yrs (P), and ±2.3 m/5yrs (H), respectively.**

•**The PPC results demonstrate that the computed RO inter-center mean time series are very useful for monitoring the quality of RO data products from individual centers.**

•**Outstanding issues will be further discussed in RO trend group**

• Shu-peng Ho[1], Doug Hunt[1], Andrea Steiner[2], Anthony J. Mannucci[3], Gottfried Kirchengast[2], Hans Gleisner[4], Stefan Heise[5], Axel von Engeln[6], Christian Marquardt[6], Sergey Sokolovskiy[1], William Schreiner[1], Chi Ao[3], Jens Wickert[5], Stig Syndegaad[4], Kent Lauritsen[4], Stephen Leroy[7], Rob Kursinski[8] ,Ying-Hwa Kuo[1], Barbara Pirscher[2], Torsten Schmidt[5], Michael Gorbunov[4], The Reproducibility of GPS Radio Occultation for Climate Monitoring: Profile to Profile Inter-comparison of CHAMP Climate Bending Angle, Refractivity, Temperature, Geo-potential Height, and Pressure Records 2002-2008 from Different Data Centers, JGR, 2012

• A. K. Steiner[1], D. Hunt[2], S.-P. Ho[2], G. Kirchengast[1], A. J. Mannucci[3], B. Scherllin-Pirscher[1, 2], H. Gleisner[4], A. von Engeln[5], T. Schmidt[6], C. Ao[3], S. S. Leroy[7], E. R. Kursinski[8], U. Foelsche[1], M. Gorbunov[4, 9], Y.-H. Kuo[2], K. B. Lauritsen[4], C. Marquardt[5], C. Rocken[2], W. Schreiner[2], S. Sokolovskiy[2], S. Syndergaard[4], and J. Wickert[6], Quantification of Structural Uncertainty in Climate Data Records from GPS Radio Occultation, GRL. 2012.